Monte Carlo simulations of complexation between weak polyelectrolytes and a charged nanoparticle. Influence of polyelectrolyte chain length and concentration.

Morten Stornes,[†] Per Linse,[‡,¶] and Rita S. Dias*,[†]

†*Department of Physics, NTNU - Norwegian University of Science and Technology, NO-7491 Trondheim, Norway*

‡*Division of Physical Chemistry, Center for Chemistry and Chemical Engineering, Lund University, S-22100 Lund, Sweden*

¶*Passed away March 24, 2017*

E-mail: rita.dias@ntnu.no

Abstract

Complexation between multiple weak polyacid chains and a positively charged spherical nanoparticle has been studied by means of Monte Carlo simulations. By considering titration curves, it is found that variations in the polyacid chain length and concentration, and the polyacid-to-nanoparticle mixing ratio influences the ionization of the system. For larger mixing ratios and longer chain lengths, the titration curves start to exhibit complex shapes with multiple inflection points. We also find that in some cases it is possible to differentiate between free and adsorbed chains, based on the charge probability distribution and the probability distribution of the gyration radius. Furthermore, the adsorption of weak polyacids has been compared with that of strong polyacids and the fraction of adsorbed monomers is found

to be slightly larger for the strong polyacids. In addition, the fraction of adsorbed chains can be much lower for the weak polyacids due to their ability to concentrate charge in few chains.

Introduction

Over the past decades, there has been a substantial amount of research done on polyelectrolytes (PEs). They have multiple industrial and commercial uses, e.g. for use as rheology modifiers in food or as flocculation agents in water treatment. In addition, they are fundamental in biological systems - important biological macromolecules such as nucleic acids, proteins and polysaccharides are polyelectrolytes. Hence, having a good understanding of how PEs interact with surfaces and other macromolecules and how polyelectrolyte complexes form, is needed to properly understand biological processes such as DNA condensation, while also having potential applications in e.g. gene and drug delivery systems. Considerable work has recently been done to understand PE-surface interactions and the formation process of PE complexes, with several reviews available. [1-9]

Part of the challenge in understanding PE complex formation and PE-surface interations, lies in the nature of the long-range electrostatic correlations inherent in polyelectrolyte systems. Unlike polymers, polyelectrolytes have acidic/basic groups which, upon deprotonation/protonation in a solution, creates electrically charged segments. These charged segments increase the complexity of the systems, making them more difficult to describe theoretically. On the other hand, this property improves the solubility of the polyelectrolytes in polar solvents due to the release of counterions and hydration effects (in water), making them highly useful in processes occurring in aqueous solutions. It also opens up the possibility to assert a certain degree of control of the PE conformation and the complexation process, by controlling e.g. the charge density or charge distribution of the PE.

Analogous to acids and bases, PEs can be divided into weak or strong. A strong polyacid will dissociate completely in solution, and have a fixed configuration of charges, while dissociation of a weak polyacid will depend on the solution pH. Weak PEs also exhibit charge mobility, where intrachain interactions will leave areas of the PE chain predisposed to disso-

2

ciation.[10] This is believed to impact the interaction between the chain and oppositely charged surfaces and enhance the formation of macroscopic complexes, when compared with strong PEs with quenched charges.[11,12] Additionally, studies on the phase behavior of polyion and surfactant micelles as a function of polyacid ionization have shown that weak polyacids are able to stabilize micellar cubic phase up to a very low fraction of charged monomers, while for quenched chains the loss of long-range order occurred at much higher fraction.[13]

In this work, we have focused on the adsorption of weak polyacids on a positively charged, spherical nanoparticle (NP). These systems can function as general representations of real systems, where e.g. the NP can be considered as a globular protein[12,14] or spherical surfactant micelles and the PE as a polypeptide.[15] A significant amount of modeling has previously been done on adsorption of strong PEs on a spherical NP. Wallin and Linse used Monte Carlo (MC) simulations to study how the PE chain flexibility,[16] linear charge density[17] and number of PEs[18] affect the complex formation. Skepö and Linse have looked at systems with one PE and multiple NPs[19,20] while Akinchina and Linse focused on the interaction between a single strong PE and NP and how the persistence length, polyion length and charge density influenced the conformational properties of the resulting complex.[21,22] Adsorption of short PE chains onto a NP[23] or Janus particle[24] have also been considered. The conformational properties for this type of system has also been studied analytically.[25,26] Stoll and co-authors have also used MC simulations in their work on weak PE-NP complexation. This includes studies on PE stiffness, NP charge density and salt in the Debye-Hückel approximation, both for one PE and NP[27] and for a single PE with multiple NPs.[28] The influence of salt and salt valency using explicit ions,[29] as well as the adsorption of a weak polyampholyte on a NP,[30] have also been addressed.

Here, we seek to expand on the previous studies, which mainly focus on single-chain systems or quenched PEs. MC simulations are used to study the effect of pH, PE chain length and concentration on PE-NP complexation, PE ionization (titration curves) and charge distribution in the system. This is useful to better understand how e.g. charged colloids may affect the properties of polyelectrolyte solutions or flocculation in NP-PE solutions, where the relative concentration of PEs and NPs can influence experimental results. It is found that the titration curves of this seemingly simple system can exhibit complex shapes given the right PE

concentration and chain length, something that, to the best of our knowledge, has not been shown previously. We also find clear differences between the charge of PE chains in the bulk and those adsorbed on the NP, and there seems to be a window of maximum chain adsorption depending on the pH and chain length.

Model

We have used a simple coarse-grained model of a single positively charged NP in a salt-free solution with several weak polyacids and counterions, as seen in Figure 1. Each polyacid chain consists of N_{mon} hard-sphere monomers which can be either negatively charged or neutral. The monomers are connected by harmonic bonds in a flexible chain, i.e. there are no angular force terms between monomers. The nanoparticle is a hard sphere with a fixed point charge, $z_{NP}e$, in the centre. z_{NP} is here the NP charge valency and e the elementary charge. Correspondingly, there are z_{NP} respective counterions to the NP to preserve overall charge neutrality. All counterions are modelled as hard spheres. The solvent is not explicitly modelled, but enters the model through the relative permittivity.

The total potential energy of the system is given by

$$U = U_{el,hc} + U_{bond}, \tag{1}$$

where

$$U_{el,hc} = \sum_{i<j} u_{ij}(r_{ij}), \tag{2}$$

is the combination of the electrostatic potential between particles and the hard-sphere repulsion, so that

$$u_{ij} = \begin{cases} \infty, & r_{ij} < R_i + R_j \\ \frac{z_i z_j e^2}{4\pi\varepsilon_0 \varepsilon_r r_{ij}}, & r_{ij} \geq R_i + R_j \end{cases}. \tag{3}$$

Here, z_i denotes the valency of particle i, r_{ij} the separation between particles i and j, and

4

ε_0 and ε_r are the vacuum and relative permittivities. The bond potential is given by

$$U_{bond} = \frac{k_{bond}}{2} \sum_i^{N_{bond}} (r_{i,bond} - r_0)^2, \tag{4}$$

with $r_{i,bond}$ being the bond length of bond i, r_0 the equilibrium separation and k_{bond} the force constant. The two latter values are set to $r_0 = 5$ Å and $k_{bond} = 0.4$ Nm^{-1}. Particles are moved by single-particle translation, full-chain translation and chain pivoting.

In addition to the previously mentioned potentials, one has to take into account the change in free energy when protonating/deprotonating monomers. The free energy of a polyacid monomer is related to the solution pH by

$$U_{prot} = k_B T \ln 10 (\text{pH} - \text{p}K_a) z, \tag{5}$$

where k_B is the Boltzmann constant, T the temperature and $\text{p}K_a = -\log(K_a)$ with K_a being the acid dissociation constant of the polyacid.[31] On deprotonation, the valency z goes from 0 to -1, reducing the free energy if pH $>$ pK_a. As the ionization of the polyacid increases, further ionization is made more difficult due to intrachain electrostatic interactions. Unlike monoprotic acids, which possess a single value for K_a, each titration site in a polyacid will have a slightly different K_a, which is dependent on the ionization of the neighbouring sites. This can be simplified by a mean field approximation, where we assume a single, apparent pK_a for all titration sites so that

$$\text{p}K_a = \text{pH} - \log\frac{\alpha}{1 - \alpha}, \tag{6}$$

where α is the average fractional ionization of the chain.[32] For a single ionized monomer ($\alpha \to 0$), pK_a equals that of a monoprotic acid, pK_0. It is common to use pH-pK_0 in eq 5 instead, and consider the difference between the apparent dissociation constant and the single-monomer constant,

$$\Delta \text{p}K = \text{p}K_a - \text{p}K_0 = \text{pH} - \text{p}K_0 - \log\frac{\alpha}{1 - \alpha}. \tag{7}$$

Thus, the potential difference that determines the probability of accepting the switching on

or off of a monomer charge is given by

$$\Delta U = \Delta U_{el} + k_B T \ln 10 (\text{pH} - \text{p}K_0)\Delta z, \tag{8}$$

where $\text{pH} - \text{p}K_0$ is given as input to the program. The average polyacid ionization, α, is calculated from the results. This is done by averaging the charge of each monomer, which itself is averaged over the entire simulation run.

Simulations are done in the canonical ensemble with $T = 298$ K and $\varepsilon_r = 78.4$. All particles are enclosed in a spherical cell of radius 300 Å, which is large enough to avoid constrains in all calculated systems. Monomers and counterions all have radii of 2 Å, and are monovalently charged, unless they are neutral. For each monomer, there is a counterion in the solution, and for each charge that is switched on or off in a monomer, there is a corresponding charge switch in a counterion to preserve charge neutrality. The NP has a radius of $R_{NP} = 20$ Å and a valency of $z_{NP} = 60$. Chains are considered adsorbed if at least one monomer is adsorbed, and monomers are considered to be adsorbed if they are within a threshold distance of $d = 6$ Å of the NP surface. This criterion is based on threshold distances used in similar systems and is within the Bjerrum length. While there are improved and more accurate threshold distances based on e.g. energy criteria, we are mainly concerned with trends here, and this simple distance-based criterion is deemed sufficient.

The simulations have been done in equilibrated systems for different $\text{pH} - \text{p}K_0$, where the polyacid chain length, N_{mon}, and mixing ratio, R, have been varied (see Table 1). The mixing ratio is defined as the ratio between the total number of monomers in the system and the NP charge valency,

$$R = \frac{N_{mon}N_{ch}}{z_{NP}}, \tag{9}$$

where N_{ch} is the number of polyacid chains. In the case of fully ionized polyacids, the mixing ratio equals the total charge ratio between polyacids and the NP. The number and size of loops, trains and tails is also calculated. Trains are defined as sequences of adsorbed monomers, while tails are non-adsorbed monomers at the end of the chain. Loops are sequences of non-adsorbed monomers which are not part of a tail, that is, they start and end with trains.

6

All simulations were performed using the MOLSIM package, v. 6.0.5.[33]

Table 1: Overview of systems studied. Values are number of chains, N_{ch}, for the given N_{mon} and R. Systems with a single 120-monomer long chain was occasionally studied as a control and for comparison with single-chain systems.

N_{mon}	R			
	0.5	1.0	1.5	2.0
4	-	15	-	30
6	5	10	15	20
10	3	6	9	12
20	-	3	-	6
30	1	2	3	4
60	-	1	-	2

Results and discussion

Titration curves

We have started by evaluating the ionization of a single polyacid in the presence of counterions only, as shown in the black dotted curves in Figures 2 and 3. Shorter chains are more easily ionized than longer ones, that is, smaller $pH - pK_0$ variations are needed to reach the same ionization degree, as previously described and can be seen in Figure 3. This is due to the increased difficulty of dissociating monomers which have neighbouring, ionized monomers, as evidenced by the fact that larger deviations from the titration curve of a single monomer (dashed grey line) occur at the higher ionization degrees. This can also be visualized in the positive ΔpK values (bottom panel in Figure 2) obtained for these systems, which increase with α.

Figure 2 shows the titration curves of 30 monomer-long chains ($N_{mon} = 30$) in the presence of a NP. At a mixing ratio of $R = 0.5$ (one chain), the ionization rate is the fastest. While the polyacid suffers from increased dissociation difficulty due to its length, this is clearly compensated by the presence of the NP and concomitant neutralization of the charged polyacid
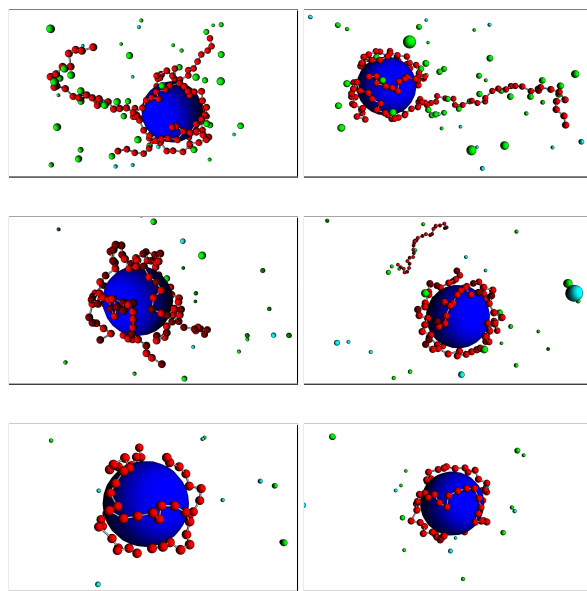
Figure 1: Example of simulated systems. Green particles are positive counterions to the red poly-acid, cyan are negative counterion to the NP. Bright red/green are charged monomers/counterion, dark red/green are neutral. Top: $R = 2, N_{mon} = 60$ at $\alpha = 1$ with tails extending from the complex. Middle: $R = 2, N_{mon} = 30$ at pH-p$K_0 = 0$ ($\alpha = 0.53$) with four chains adsorbed (left) and pH-pK_0 = 2 ($\alpha = 0.81$) with three of four chains adsorbed (right). Bottom: Example of conformations for two chains with $N_{mon} = 30$ in a tennis ball-like structure. One system has one fairly straight chain and a chain bending twice, forming two semicircles (left) while the other has both chains forming a semi circle each (right).
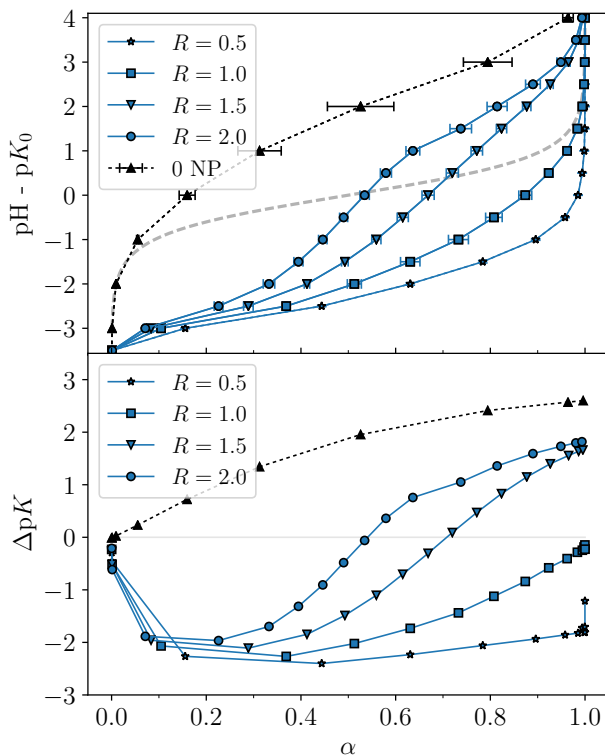
Figure 2: Titration curves showing the increase in ionization with pH (top) and the difference between the apparent and intrinsic dissociation constant (bottom) for increasing ionization in systems with $N_{mon} = 30$ at different mixing ratios. Dashed grey lines show the titration curve of a solution of single monomers, here calculated by $pH - pK_0 = \log[\alpha/(1 - \alpha)]$, which fits with control simulations of a single monomer solution. The addition of a NP increases the dissociation of the monomers, but the effect decreases with increasing polyacid concentration.

monomers. In addition, ΔpK is negative for all $\alpha \in (0, 1.0)$, indicating that the polyacid ionizes faster than single monomers in a solution with no NP. Such shift in the pK_a of the weak polyacid in the presence of a NP has been previously described, as mentioned in the introduction.[5] As the mixing ratio is increased, by increasing the number of polyacid chains, the polyacid ionization becomes slower and the shape of the titration curves changes as well. At the lower mixing ratios, the curves have an overall shape similar to that of a single chain or a single-monomer solution, with the curves seemingly just shifted downwards. As the mixing ratio increases, the shape changes noticeably. Compared to the single monomer solution, the
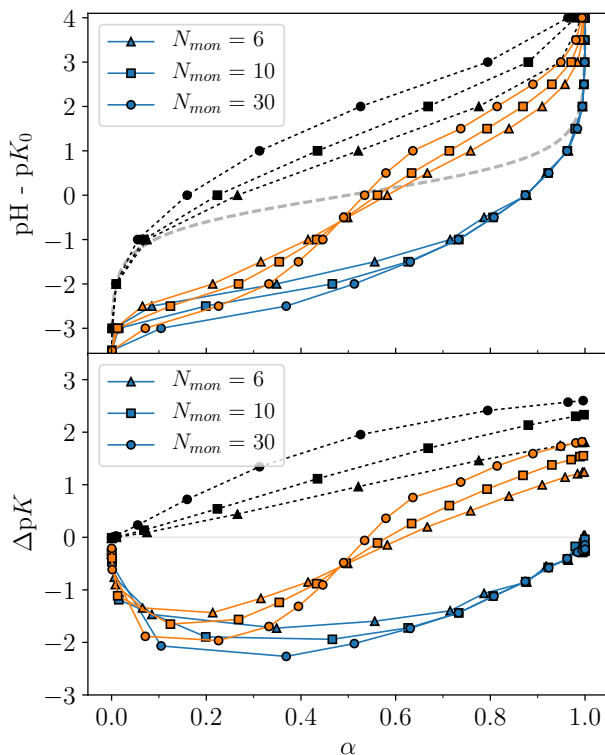
Figure 3: Titration curves and ΔpK for different chain lengths with 0 NP (dotted black lines), $R = 1$ (blue lines) and $R = 2$ (solid orange lines) are plotted. The shape of the titration curve depends on the chain length as well as the mixing ratio. The ionization rate also differs between chain lengths, with shorter chains ionizing faster when free, while longer chains tend to ionize faster in the presence of the NP in certain scenarios. Errorbars excluded for increased readability.

ionization is faster for any system with $R \leq 1.0$, as evidenced by $\Delta pK < 0$ for these systems (Figure 2). This holds true for all the systems studied, with N_{mon} ranging from 4 (see Figures S1 and S2) to 60. For $R > 1.0$, the ionization slows down at larger α, and ΔpK becomes positive at or after the isoelectric point, i.e. for $\alpha \geq 1/R$, depending on the chain length. ΔpK can also become positive before the isoelectric point in systems where the NP-polyacid interaction is screened, e.g. by including salt in the solution.[27,29] This polyacid ionization behaviour strongly suggests the independent titration of adsorbed and non-adsorbed polyacid chains.

The ionization of the polyacid is also dependent on the chain length which can be altered either by adjusting the monomer-monomer distance, or by changing the number of monomers.

It has previously been shown that for a single, free, PE, an increase in the monomer-monomer distance promotes the PE ionization,[10] whereas increasing the number of PE monomers will reduce the ionization rate.[27] In our study, the monomer-monomer distance has been fixed, and only N_{mon} is changed. We find that, while the shorter chains ionize more easily than the long chains when the PEs are free, the opposite is true in the presence of a NP. Figure 3 shows that the longer chains ionize faster for $R = 1$ (blue lines with circles), up to $\alpha \sim 0.7$ where the curves converge. At low pH, the ionized monomers will belong mainly to adsorbed chains. Systems with short chains have a larger fraction of free chains when compared to systems with longer chains, hence having fewer monomers close to the NP surface, and a lower ionization rate.

At $R = 2$ (orange lines), the effect of chain length on the shape of the titration curve is further highlighted. While for shorter chains (e.g. $N_{mon} = 6$) the titration curve is nearly straight, longer chains show multiple inflection points, with the shape being reminescent of a polyacid with multiple acidic groups with different dissociation constants, rather than the simplified model with $K_a = K_0$ for all monomers that is used here. This is particularly evident for $N_{mon} = 30$ at $R = 2.0$ (orange, circular markers in Figure 3). Such titration behaviour has not been described before, although there is a hint of this shape for the flexible chains in Figure 10 in Ulrich et. al.,[27] where the influence of chain stiffness on the titration curve is investigated. The shape of the titration curve seems thus to be particular to systems with long and flexible chains in sufficient number to overcharge the NP. As there is an increased concentration of monomers around the NP (as discussed later), the ionization rate decreases until chains are expelled from the complex. Such decrease in the monomer density around the NP further enhances the ionization of adsorbed monomers, and, again, highlights the presence of two populations: NP-associated and free polyacid chains.

Since longer chains ionize faster than short ones in the presence of the NP and chain ionization is more difficult for longer chains, overlaying the titration curves for systems with different chain lengths and $R = 2$ (orange lines), shows a crossover in the titration curves by the isoelectric point. Such crossover is observed also in systems with $R = 1.5$ (Figure S1). Solutions with shorter chains reach positive ΔpK at higher α (≈ 0.65 for $N_{mon} = 4$, as opposed

to $\alpha \approx 0.54$ for $N_{mon} = 30, 60$). It should be mentioned that increasing the chain length of the polyacid beyond 30 monomers does not affect the titration curves much, and that the titration curves for a system of 2×60 monomers and 1×120 monomers essentially overlap (Figure S3). The presence of free polyacid chains is thus not required to observe such complex titration curve, but the chain needs to be sufficiently long so that the non-adsorbed part of the chain behaves as a free one. This is not the case with, for example, $N_{mon} = 30$ and $R = 1.5$.
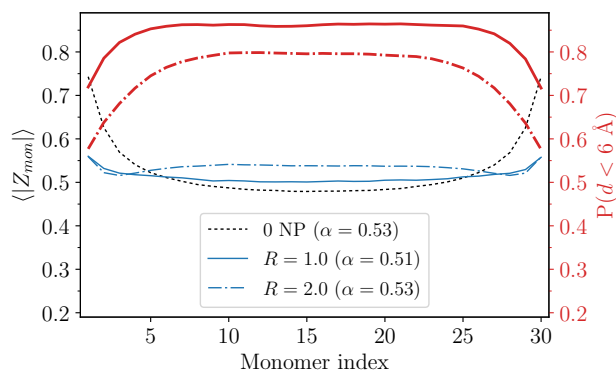
Polyacid charge profile

Figure 4 shows the charge distribution along the polyacid chain for a few selected systems. Note that each graph in this figure compares polyacids with similar ionization degree (α) and, consequently, different $pH - pK_0$ values. In the absence of a NP (dotted black curves), the charge mobility in weak polyelectrolytes induces the concentration of charge of partially ionized chains towards the ends of the chains, due to the intrachain electrostatic repulsion, as shown previously.[10]

The addition of a NP to the system reduces the difference in the charge distribution along the polyacid chain (blue curves), which can be rationalised by looking at the contact probability profiles (red curves). Independently of polyacid chain length or ionization degree, the polyacid-NP contact probability decreases towards the end of the polyacid due to the increased entropy of the ends of the chains and weaker electrostatic attraction to the NP. Since the central part of the polyacid chain has a higher probability of being found close to the NP, this polyacid-NP contact further increases the ionization of the monomers to minimize the energy, leading to the more uniform distribution of charge in NP-associated polyacids. Generally, the charge profile of the polyacid chain has a minimum in the center, with increasing charge towards the ends of the chain as in Figure 4a. However, depending on the degree of ionization, chain length and mixing ratio, the charge profile can also adopt two minima near the ends of the chain, with local maxima near the middle and at both ends, as shown in Figure 4b (dash-dotted line). This charge profile is more prevalent for longer chains at larger mixing ratios and is due to the increased monomer density in vicinity of the NP. As discussed, the center of the chain has a higher probability of being in contact with the NP (red curves in Figure 4). With increasing
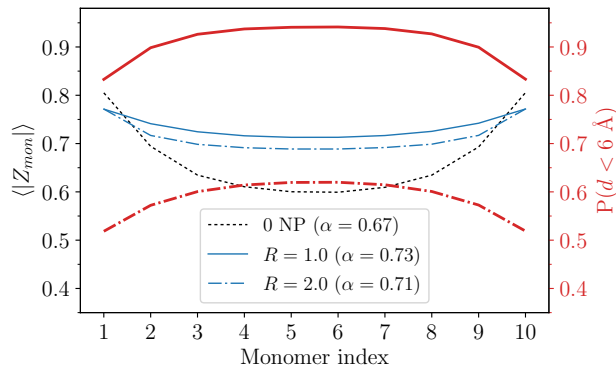
(a)

(b)

Figure 4: Charge and contact profiles of polyacid monomers for systems with similar ionization degree of $N_{mon} = 10$ (a) and $N_{mon} = 30$ (b). Black, dotted curves show the average charge of each monomer in a system with no NP. Blue curves show the average monomer charge in systems with a NP at different mixing ratios. Thick, red curves show the adsorption probability for polyacid adsorption on the NP at a threshold distance of 6 Å. Fluctuations are small, and errorbars are excluded for increased readability.

mixing ratios above neutralization, the contact probability is generally reduced. For the shorter chains, this is due to a larger amount of free chains in the bulk, while the longer chains adopt long tails extending from the NP, as the area around the NP becomes crowded with monomers. Such tails are less likely to be charged as they are not in contact with the NP but, due to the charge mobility and intrachain repulsion, the ends tend to have a larger charge than the rest of the tail. The longer tails and, consequently, the lowering of the monomer ionization close to (but not at the) ends, gives rise to the charge profile with two minima.

Due to the short chain lengths used here, as compared to the NP size, the charge profiles in Figure 4 do not fluctuate much between the ends. For longer chain lengths ($N_{mon} = 60$), there is more fluctuation in the contact probability, with asymmetric profiles developing for the charge profile and contact probability at larger R and pH (see discussion below).

Since the chain possesses a mirror symmetry, the monomer adsorption also reflects this property, somewhat disguising the effect.

By defining $\Delta Z = Z_{end} - Z_{mid}$, we see how the charge difference between the tails and the center of the adsorbed chain changes with α^{ads}, the ionization degree of the adsorbed chains only (Figure 5). Here, Z_{end} is the average charge of the end monomers of the chain, and Z_{mid} the average charge of the two monomers in the middle of the chain, taking into account the mirror symmetry of the chain. For the system with no NP (black dotted curve), the ends always have a larger charge than the center, except for fully ionized or neutral chains, and the difference reaches its maximum around $\alpha = 0.5$. For the polyacids adsorbed on the NP, ΔZ is much smaller, and negative at $\alpha^{ads} \approx 0.2 - 0.3$. This is indicative of a slightly larger charge near the center of the chain, which also has a higher contact probability, as discussed above. As the ionization of the adsorbed polyacids increases, the polyacid ends will have a higher charge on average due to the intrachain repulsion and charge mobility, which is a similar behaviour as that observed for free polyacids. The difference in charge between the tails and center of the polyacid shifts down in the middle range for increased mixing ratios. Central monomers have more intrachain neighbours than tail monomers. As the polyacid concentration is increased, the tail monomers will receive more interchain neighbours relative to the central monomers. The system discussed here is for $N_{mon} = 30$, but the results also hold for $N_{mon} = 60$. Shorter

chains have not been considered. Additional information on the charge profile is given in the supplementary materials and Figure S4.
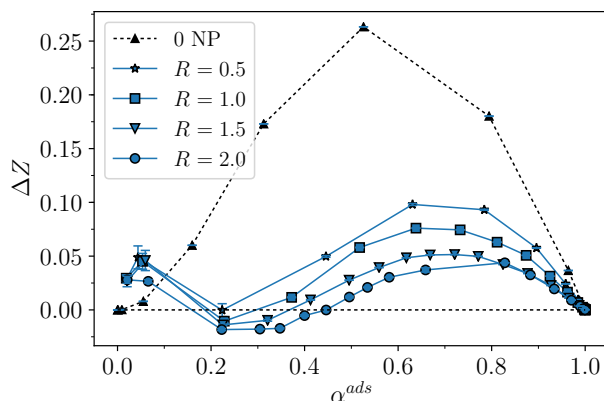

Figure 5: Charge difference ΔZ between end and mid monomers of adsorbed polyacid chains for $N_{mon} = 30$. α^{ads} denotes the average ionization of adsorbed chains only, except for the case of 0 NP.

Polyacid charge probability distributions

Figure 6 gives the charge probability distribution for polyacids in a few different systems for increasing pH–pK_0. As expected, the distribution shifts for larger values as the pH is varied and, concomitantly, the degree of ionization of the chains increases. Of particular interest here are the bimodal distributions that are evident for intermediate values of α (e.g. solid blue curves in Figure 6). This is indicative of two different populations of polyacids – adsorbed chains which are more easily ionized at the surface of the NP, and free chains with fewer charges. The bimodal distributions are more evident in systems with (i) low ionization, (ii) larger mixing ratios and, (iii) shorter chains. Observation (i) is attributed to the concentration of the few charges in one or few chains that adsorb to the NP while leaving the other chains close to neutral. Also in (ii), the charges can be concentrated in the number of chains needed to neutralize the NP, leaving the excess in solution and preserving less charge. Finally, obser- vation (iii) is a consequence of the weaker electrostatic attraction of the shorter polyacids to the NP, which typically leads to a relatively large population of chains free in solution even

15

below the charge neutrality point, as can also be seen for PE complexes.[34] The lower connectivity of short polyacid chains also grants the system a larger mixing entropy, which opposes adsorption, and may also lead to a more even distribution of adsorbed chains on the NP surface, hindering adsorption of free chains, even though there is some exchange. As the NP also promotes ionization of the adsorbed polyacid, this gives rise to two distinct populations.

Polyacid adsorption indicators and NP overcharging

Figure 7 shows some monomer and chain indicators as a function of $pH - pK_0$ for systems at $R = 2$. These show that when the polyacids are sufficiently charged, the systems exhibit overcharging and charge inversion of the polyacid-NP complex; the thin dotted line in Figure 7a indicates charge neutrality for a fully charged chain. The charge excess is dependent on chain length, and the complexes formed with the shortest chains ($N_{mon} = 4$) show little to no overcharge.

Figure 7a, in particular, shows N_{mon}^{ads}/N_{mon} as a function of $pH - pK_0$ for three different chain lengths and $R = 2.0$ (blue curves). As the $pH - pK_0$ (and α) increases, N_{mon}^{ads} increases, reaching a maximum around $pH - pK_0 \approx 0.0 - 0.5$ ($\alpha \approx 0.56 - 0.58$). For $N_{mon} = 10$, it stays constant, while for $N_{mon} = 30$ and 60 it decreases from a maximum of approximately 90 adsorbed monomers on average to ≈ 78.5 adsorbed monomers, giving a charge ratio of ≈ 1.3. This is more clearly seen in Figure 8a, where the charge ratio of adsorbed monomers and the NP, $\beta = N_{mon}^{ads}/z_{NP}$, is plotted as a function of N_{mon} at $\alpha = 1$ for $R = 1.0$ and 2.0. It should be noted that there is no difference in the number of adsorbed monomers at high $pH-pK_0$ between $R = 1.5$ and 2. Shorter chains are not able to create an overcharged complex to the same degree, and for the shortest chains ($N_{mon} = 4$), β reaches the maximum at around 0.95. For systems with $R = 1$, the polyacid chains tend to neutralize the NP charge, with β ranging from ≈ 0.90 ($N_{mon} = 4$) to ≈ 0.98 ($N_{mon} = 60$) at $\alpha = 1$ (Figure 8a). Here, $\beta < 1$ due to the adsorption threshold of 6 Å; a higher threshold would have given $\beta = 1$. In systems with $N_{mon} \geq 6$, all chains adsorb at larger pH for $R = 1$, creating a neutral complex, but in systems with 4 monomer-long chains, one chain will often be desorbed from the NP.

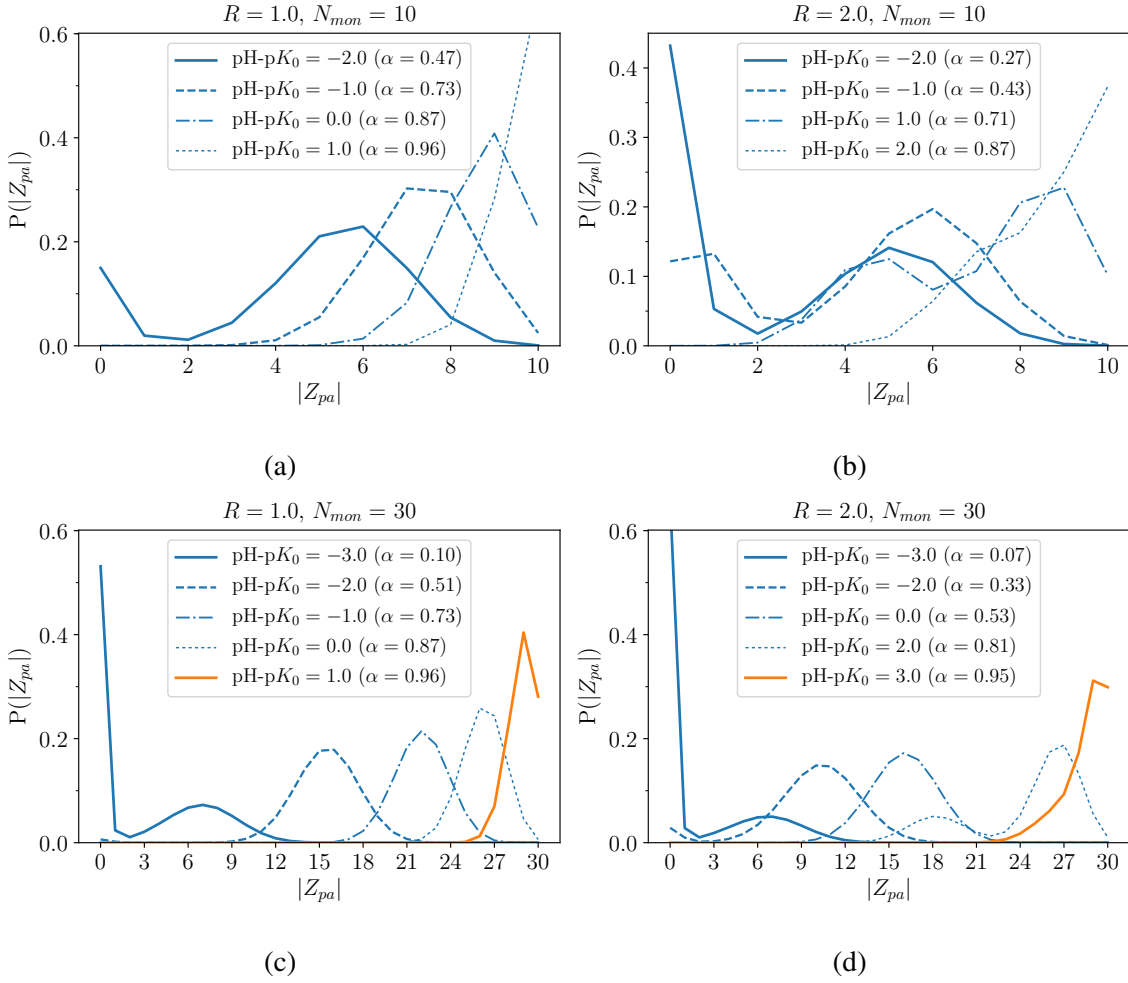Figure 6: Charge probability distribution of polyacid chains at selected pH-pK_0 values. For $N_{mon} =$ 10 at $R = 1.0$ (a) and $R = 2.0$ (b) and $N_{mon} = 30$ at $R = 1.0$ (c) and $R = 2.0$ (d). The shape of the distributions depends on the charge difference between free and adsorbed chains. At α close to 0/1, the polyacid chains are mostly neutral/charged, giving a unimodal distribution. The bimodal distributions are clearer at intermediate values of α in the systems with multiple free chains, as in (b). In (d), the system changes from having free chains at small α, to all chains adsorbed at intermediate α and to again having free chains at large α. This gives rise to a unimodal distribution for $\alpha = 0.53$, while systems with larger and lower ionizations exhibit (signs of) a bimodal distribution.
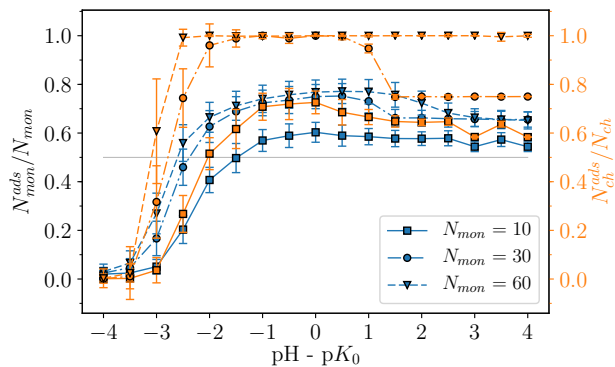
(a)
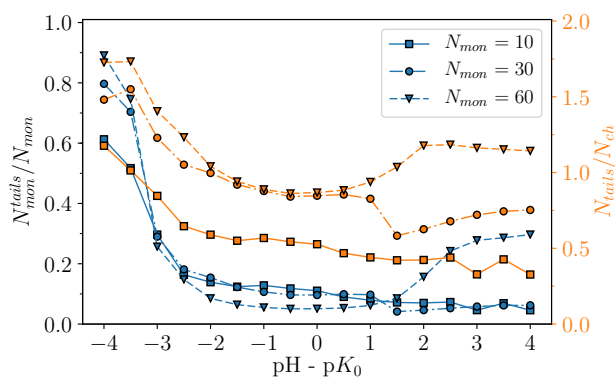
(b)

Figure 7: (a) Fraction of adsorbed monomers (blue) and adsorbed chains (orange) for $R = 2$. The gray line indicates where the number of adsorbed monomers equals the charge valency of the NP. (b) Fraction of monomers in tails per chain (blue) and number of tails per chain (orange) for $R = 2$. Errorbars in the bottom panel are excluded for increased readability but fluctuations are close to ± 0.2 and ± 0.5 for the fraction of monomers in tails per chain and the number of tails per chain, respectively.
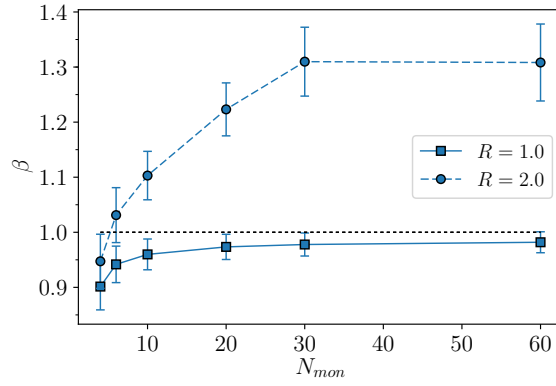
(a)
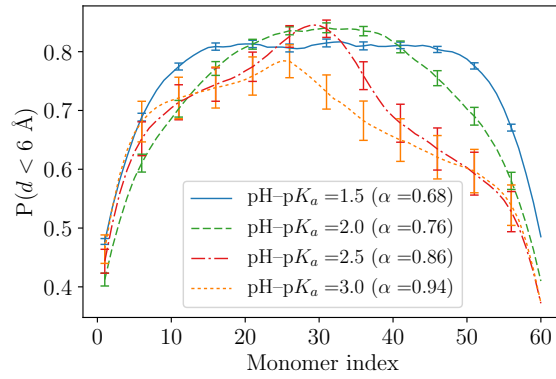
(b)

Figure 8: (a) Ratio between adsorbed monomers (N_{mon}^{ads}) and NP valency (z_{NP}), β, as function of chain length at $\alpha = 1$ for different mixing ratios. (b) Monomer adsorption probability in a system with $N_{mon} = 60$, $N_{ch} = 2$. For clarity, errorbars are only shown for every fifth monomer index.

Figure 7a shows, in addition, the fraction of adsorbed chains N_{ch}^{ads}/N_{ch} (orange curves). While the systems with $N_{mon} = 30$ and 60, for $R = 2$, have the same number of adsorbed monomers when the system is fully ionized, the number of adsorbed chains differs. For $N_{mon} = 30$, one of the four chains is excluded from the NP at $pH - pK_0 = 1.5$ due to the strong electrostatic repulsion between adsorbed chains as their ionization increases. This reduces the number of adsorbed monomers slightly, but the adsorbed chains become more tightly packed on the NP, as seen by the decrease of monomers in loops and increase of monomers in trains (Figure S5). For $N_{mon} = 60$, the reduction in adsorbed monomers is more gradual, as both chains remain adsorbed at high pH. The reduction in N_{mon}^{ads} is, in this case, rather due to tails protruding from the NP-polyacid complex due to, again, electrostatic repulsion between adsorbed chains (Figure 7b). The tails grow both in length (blue curve with triangles) and number (orange curve with triangles) as the ionization increases further.

To summarize, there is a window of pH values where there is a maximum number of chains and monomers adsorbed. As seen in Figure 7a, this window lies around the isoelectric point (e.g., $\alpha = 0.5$ for $R = 2$) and is smaller for shorter chains.

Figure 8b shows the contact probability distribution for increasing pH. While the tail size/number of tails starts to increase from $pH - pK_0 = 1$ (Figure 7b), the contact probability distribution is symmetrical, but with increasing fluctuations at the ends of the chains, up to $pH - pK_0 = 2.2$ ($\alpha = 0.80$, not shown). This indicates a fluctuating multi-tail state up until this point, whereafter the system begins to display predominantly one long tail, as evidenced by the reduced contact probability for the ends, increased fluctuations and emerging asymmetric profiles. The latter is due to the equilibration time of the system, and arises with relatively short simulation runs. This will average out over longer runs due to the chain symmetry. Such behaviour of tail extension has been shown previously, both analytically[35] and by MC simulations,[22,23] for the complexation between a single strong PE and NP. The mentioned studies show a single tail extending from the complex when the PE is longer than a critical length, and a fluctuating two-tail state has been described for flexible PEs.[22] In the system studied here, e.g. as seen in Figure 1, multiple tails (2-3) composed of several monomers are occasionally observed (top left image) at $\alpha = 1$. Mostly though, the system is confined to a single long

tail with one or two small tails composed of a single monomer or two (top right image), even though the system is composed of two polyacids and can potentially have four longer tails. This is in line with previous results. [22]

The overcharging of complexes as calculated here, does not take into account the interaction with counterions which will invariably adsorb/condense on the complex and, to some extent, screen it from other charged particles. The counterion-polyacid radial distribution function for increasing R for $N_{mon} = 30$ can be seen in Figure S6.

As mentioned in the introduction, weak PEs are believed to interact more strongly with NPs and give rise to more ordered structures, due to the mobility of the charges along and between the chains and potential formation of strongly charged patches along the PEs. To assess this, we have compared the adsorption between strong and weak polyacids on the NP. The strong polyacids were described in two ways: (i) strong homopolymers, where each monomer has a fractional charge equal to α, and (ii) regular strong polyacids, where α is decided by alternating sequences of fully charged or neutral monomers. Figures 9a and b show the fraction of adsorbed monomers (blue curves) and chains (orange curves) as a function of α, for systems with $N_{mon} = 30$ and 60, respectively. Our results show that strong polyacids tend to bind more strongly to the NP, in the form of both more monomers and chains adsorbed, independently of the chosen architecture (homopolymer vs. regular copolymer). The difference is especially large for the number of adsorbed chains at low α and $\alpha \sim 0.7$, but this can be attributed to the different populations of weak polyacids, with charge patches on the adsorbed polyacids and fully neutral free chains, that is, to the ability of the annealed system to concentrate charges in a few adsorbed chains, while expelling others from the NP-polyacid complex. It should be noted, however, that weak PEs show fewer adsorbed monomers than the strong PEs also for systems where all chains are adsorbed ($N_{mon} = 60$ or 120). We also find a larger number of monomers in loops in the annealed systems (not shown), which explains why we have less adsorbed monomers in these systems; the annealed PEs seem to be able to concentrate the charged monomers at the surface of the NP more efficiently than the quenched ones.

These results are in apparent disagreement with previous reports on similar systems, which describe that weak PEs have a stronger binding affinity to oppositely charged surfactant mi-
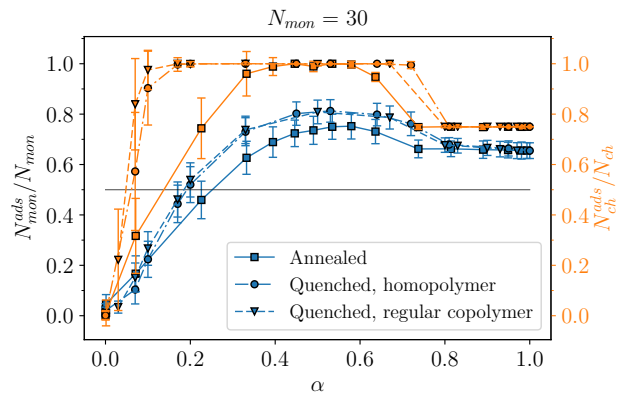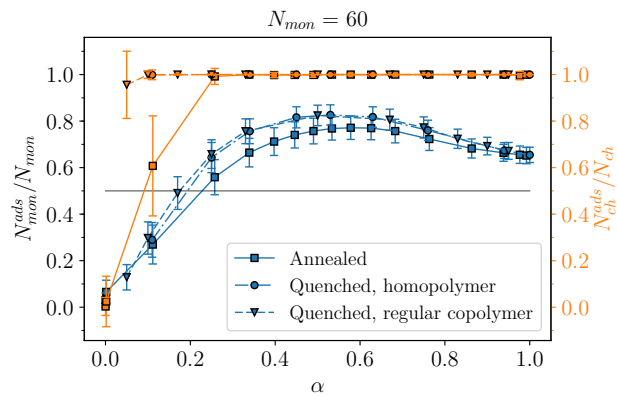
Figure 9: Fraction of adsorbed monomers and chains as a function of α for systems with annealed and quenched polyacids for $R = 2$ with (a) $N_{mon} = 30$ and (b) $N_{mon} = 60$. For the quenched polyacids, homopolymers with an equal, fractional, charge per monomer and regular copolymers, with alternating charged and neutral monomers, are checked.

celles than strong PEs, and where it is concluded that the charge mobility of long, weak, and relatively stiff PEs promotes the binding to a NP.[12] We suggest that the difference in behaviour arises from the different flexibilities of the studied PEs. For the mentioned (neutral monomer) loops to form, the chains must be flexible enough. When PEs become sufficiently rigid so that the number of contacts between the chains and the NP is reduced, the ability to concentrate charges in the adsorption points does effectively increase the number of adsorbed monomers, when compared with PEs with a quenched distribution of charge (see Figure 6 in Cooper et. al.[12]). It should also be mentioned that an increased number of adsorbed monomers onto one NP does not necessarily imply an easier formation of macroscopic NP aggregates or formation of more regular concentrated phases. In order to assess such effects, systems containing more than one NP must be taken into account.

Polyacid conformational behaviour

While only chains of length $N_{mon} = 60$ are long enough to wrap around the NP, we see tennis ball-like conformations for $N_{mon} = 30$ and 60 for highly charged chains at $R = 1$. This is similar to what has been previously reported for flexible PE chains.[21–23,27,30] The tennis ball conformation starts to be visible around $pH - pK_a = 0.5$ ($\alpha \approx 0.8$). For $N_{mon} = 30$, this is seen as the two chains either wrap in two semicircular arrangements, each forming half of the tennis ball structure, or longer, straighter chains with a bend at the end (Figure 1). At $N_{mon} = 20$, the structure is still reminescent of the tennis ball with more openings, while for $N_{mon} = 10$ and shorter, the structure disappears as the polyacids are more evenly distributed on the NP. At $R = 2$, the tennis ball conformation seems to persist, albeit with more crowding of the polyacids.

The gyration radius (R_G) of polyacids in the absence and presence of the NP has been also evaluated. In the absence of a NP, R_G increases with the polyacid ionization due to intrachain electrostatic repulsions and counterion release. This is also generally the case for shorter polyacids in the presence of the NP, as seen in Figure 10a for $N_{mon} = 30$. However, due to the interaction with the NP, the size of the polyacid does not increase much beyond 20 Å, the radius of the NP. As the ionization increases, the distribution becomes much narrower, indicating

a complete wrapping around the NP, which is also the case for $N_{mon} = 60$ (Figure 10b).

Since adsorbed polyacids have a gyration radius limited by the curvature of the NP, it is possible to distinguish between free and adsorbed polyacids for long enough chains, depending on the pH of the system. For the systems studied here, adsorbed polyacids with $N_{mon} \geq 10$ are distinguishable from free polyacids, based on R_G, while for $N_{mon} < 10$, the chains have a comparable size to the NP dimensions and thus it is not possible to distinguish the two populations (see Figure S7). Clearly, the longer the polyacid chains, the more well separated the adsorbed and free populations are. On the other hand, such distinct populations are solely observed for sufficiently large values of α; see, for example, the $P(R_G)$ evaluation as $\alpha \to 1$ in Figure 10c. This is so, because ionization at lower α is not strong enough to sufficiently extend the free polyacids. It should be mentioned that, for $N_{mon} = 60$, the distinct peaks at large α (Figure 10d) are due to the presence of long tails rather than free chains, as seen in Figures 7 and 1. Hence, this peak is centered at a smaller R_G than that for a free NP, as opposed to the systems $N_{mon} = 20$ and 30, where the respective shoulder and peak are located close to the R_G of free polyacid.

Here, and for simplicity, systems were calculated in the absence of salt. While experimental systems will invariably contain salt, we do not think the general results and conclusions will be influenced by small to moderate concentrations of salt. At large ionic concentration the electrostatic interactions will be screened, decreasing the attraction and adsorption of chains to the NP, and monomer-monomer repulsion. The titration curves will converge to that of a single-monomer solution.

Conclusion

The competition between polyacid-NP attraction and both intra- and interchain repulsion, can give rise to complex titration curves resembling systems with multiple acidic groups with different dissociation constant, even though the model assumes the same dissociation constant for all monomers. For this to happen, the polyacid chains need to be long enough to allow for both sufficient monomer density at the NP surface in a pH-region around the isoelectric point,
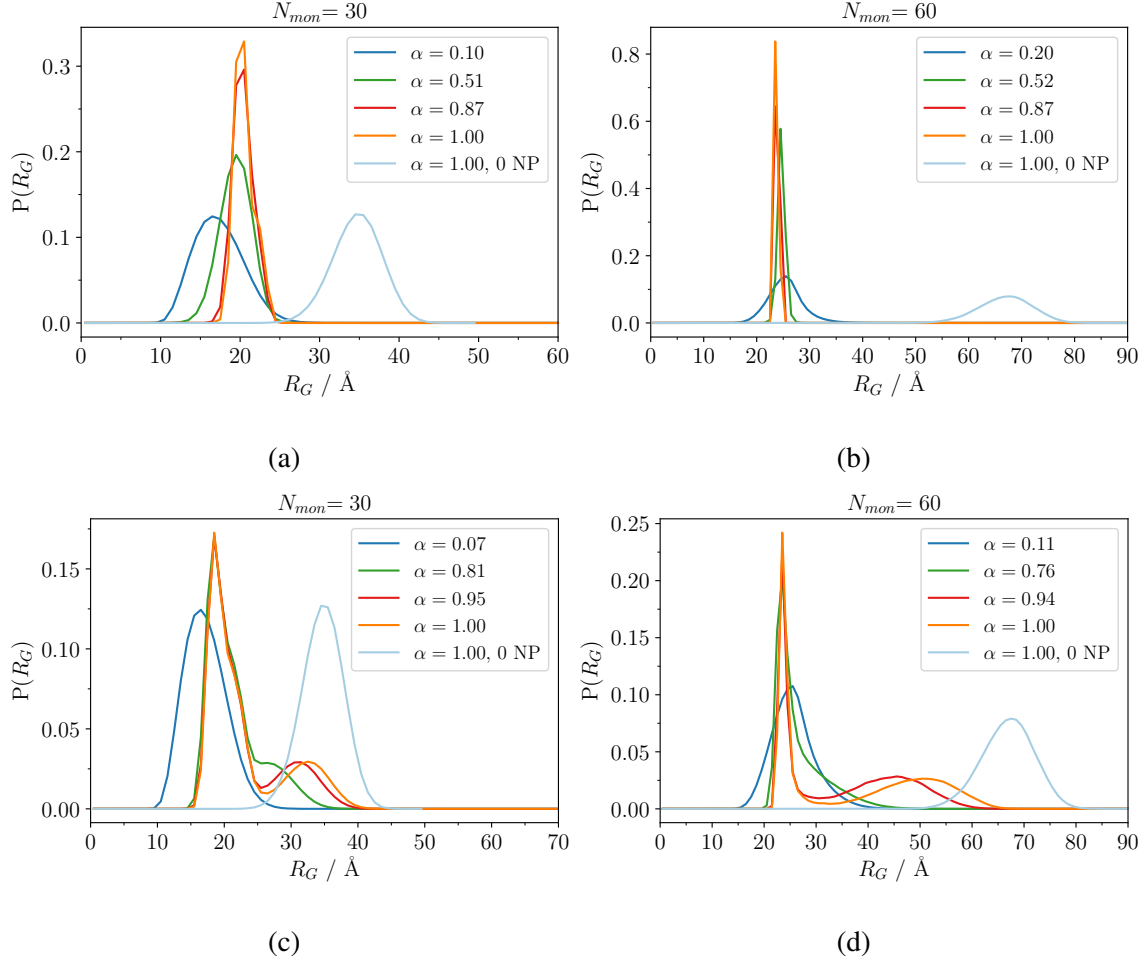
Figure 10: Probability distribution of the gyration radius R_G at different degrees of ionization. (a)-(b) display results for systems with mixing ratio $R = 1$ at $N_{mon} = 30$ and 60, respectively. (c)-(d) show results for $R = 2$. As the ionization increases, so does R_G. At $R = 2$, bimodal distributions appear at large enough ionization degrees, due to the difference between adsorbed chains which are packed around the NP and either free chains (for $N_{mon} = 30$) or adsorbed chains with long tails (for $N_{mon} = 60$).

and sufficient overcharging of the complex at high pH. The electrostatic repulsion between charged monomers then gives rise to either free chains in the bulk at high pH, or long tails protruding from the polyacid-NP complex into the bulk, which effectively behave as a free chain. Whereas shorter chains tend to have more free chains in the bulk at high pH, creating more compact complexes, long chains can form large tails, which could potentially lead to NP aggregation and precipitation.

The potential for a large monomer density around the NP close to neutralization also gives rise to a pH-dependent window of maximum chain adsorption. The window tends to be smaller for shorter chains, which have a higher adsorption threshold and are unable to overcharge the complex to the same degree as longer chains.

Systems with weak charges are able to concentrate charge in a few adsorbed chains while nearly neutral chains remain free in solution. This leads to a significantly lower fraction of adsorbed chains, specially in systems with low ionization and for slightly overcharged systems, when compared to systems calculated with strong (quenched) PEs. The number of adsorbed monomers was found to be slightly lower than in systems with quenched charges.

Two properties can be used to distinguish between free and adsorbed polyacid chains. At intermediate pH values, one can use the charge probability distribution, at least in theory, to distinguish free chains from those which are part of the polyacid-NP complex, which typically have a larger degree of dissociation. This is especially useful for shorter chains and larger mixing ratios, where there are multiple free chains. In addition, the radius of gyration shows a clear difference between free and adsorbed polyacids. Unlike the charge probability distribution, R_G can mainly be used on longer chains at large α. As the ionization increases, the free chains will go from a globular to an extended conformation. This gives a larger gyration radius as compared to chains adsorbed on the NP, which will be limited by the NP curvature.

Supporting information

Supporting information is available, containing titration curves of additional systems, more details regarding polyacid charge profile and gyration radii.

References

(1) Netz, R. R.; Andelman, D. Neutral and charged polymers at interfaces. *Physics Reports* **2003**, *380*, 1 – 95.

(2) Dobrynin, A. V.; Rubinstein, M. Theory of polyelectrolytes in solutions and at surfaces. *Progress in Polymer Science* **2005**, *30*, 1049–1118.

(3) Cooper, C. L.; Dubin, P. L.; Kayitmazer, A. B.; Turksen, S. Polyelectrolyte-protein complexes. *Current Opinion in Colloid and Interface Science* **2005**, *10*, 52–78.

(4) de Vries, R.; Stuart, M. C. Theory and simulations of macroion complexation. *Current Opinion in Colloid and Interface Science* **2006**, *11*, 295–301.

(5) Ulrich, S.; Seijo, M.; Stoll, S. The many facets of polyelectrolytes and oppositely charged macroions complex formation. *Current Opinion in Colloid and Interface Science* **2006**, *11*, 268 – 272.

(6) Borkovec, M.; Papastavrou, G. Interactions between solid surfaces with adsorbed polyelectrolytes of opposite charge. *Current Opinion in Colloid and Interface Science* **2008**, *13*, 429–437.

(7) Kayitmazer, A. B.; Seeman, D.; Minsky, B. B.; Dubin, P. L.; Xu, Y. Protein-polyelectrolyte interactions. *Soft Matter* **2013**, *9*, 2553–2583.

(8) Grosberg, A. Y.; Nguyen, T. T.; Shklovskii, B. I. The physics of charge inversion in chemical and biological systems. *Reviews of Modern Physics* **2002**, *74*, 329–345.

(9) Xiao, J.; Li, Y.; Huang, Q. Application of Monte Carlo simulation in addressing key issues of complex coacervation formed by polyeletrolytes and oppositely charged colloids. *Advances in Colloid and Interface Science* **2017**, *239*, 31–45.

(10) Ullner, M.; Jönsson, B.; Söderberg, B.; Peterson, C. A Monte Carlo study of titrating polyelectrolytes. *Journal of Chemical Physics* **1996**, *104*, 3048–3057.

(11) Yoshida, K.; Dubin, P. L. Complex formation between polyacrylic acid and cationic/nonionic mixed micelles: Effect of pH on electrostatic interaction and hydrogen bonding. *Colloids and Surfaces A: Physicochemical and Engineering Aspects* **1999**, *147*, 161 – 167.

(12) Cooper, C. L.; Goulding, A.; Kayitmazer, A. B.; Ulrich, S.; Stoll, S.; Turksen, S.; Yusa, S.; Kumar, A.; Dubin, P. L. Effects of polyelectrolyte chain stiffness, charge mobility, and charge sequences on binding to proteins and micelles. *Biomacromolecules* **2006**, *7*, 1025–1035.

(13) Norrman, J.; Lynch, I.; Piculell, L. Phase behavior of aqueous polyion-surfactant ion complex salts: Effects of polyion charge density. *The Journal of Physical Chemistry B* **2007**, *111*, 8402–8410.

(14) Carlsson, F.; Linse, P.; Malmsten, M. Monte Carlo simulations of polyelectrolyte-protein complexation. *Journal of Physical Chemistry B* **2001**, *105*, 9040–9049.

(15) Carnal, F.; Clavier, A.; Stoll, S. Polypeptide-nanoparticle interactions and corona formation investigated by Monte Carlo simulations. *Polymers* **2016**, *8*, 203.

(16) Wallin, T.; Linse, P. Monte Carlo Simulations of Polyelectrolytes at Charged Micelles. 1. Effects of Chain Flexibility. *Langmuir* **1996**, *12*, 305–314.

(17) Wallin, T.; Linse, P. Monte Carlo Simulations of Polyelectrolytes at Charged Micelles. 2. Effects of Linear Charge Density. *The Journal of Physical Chemistry* **1996**, *100*, 17873–17880.

(18) Wallin, T.; Linse, P. Monte Carlo simulations of polyelectrolytes at charged hard spheres with different numbers of polyelectrolyte chains. *Journal of Chemical Physics* **1998**, *109*, 5089–5100.

(19) Jonsson, M.; Linse, P. Polyelectrolyte-macroion complexation. I. Effect of linear charge density, chain length, and macroion charge. *Journal of Chemical Physics* **2001**, *115*, 3406–3418.

(20) Skepö, M.; Linse, P. Complexation, Phase Separation, and Redissolution in Polyelectrolyte-Macroion Solutions. *Macromolecules* **2002**, *36*, 508–519.

(21) Akinchina, A.; Linse, P. Monte Carlo simulations of polyion-macroion complexes. 1. Equal absolute polyion and macroion charges. *Macromolecules* **2002**, *35*, 5183–5193.

(22) Akinchina, A.; Linse, P. Monte Carlo simulations of polyion-macroion complexes. 2. Polyion length and charge density dependence. *Journal of Physical Chemistry B* **2003**, *107*, 8011–8021.

(23) Chodanowski, P.; Stoll, S. Polyelectrolyte adsorption on charged particles in the Debye-Huckel approximation. A Monte Carlo approach. *Macromolecules* **2001**, *34*, 2320–2328.

(24) de Carvalho, S. J.; Metzler, R.; Cherstvy, A. G. Critical adsorption of polyelectrolytes onto charged Janus nanospheres *Physical Chemistry Chemical Physics* **2014**, [*16*], *15539-15550*

(25) Schiessel, H.; Buinsma, R. F.; Gelbart, W. M. Electrostatic complexation of spheres and chains under elastic stress. Journal of Chemical Physics **2001***, 115, 7245–7252.*

(26) Schiessel, H. Charged rosettes at high and low ionic strengths. Macromolecules **2003***, 36, 3424–3431.*

(27) Ulrich, S.; Laguecir, A.; Stoll, S. Complexation of a weak polyelectrolyte with a charged nanoparticle. Solution properties and polyelectrolyte stiffness influences. Macromolecules **2005***, 38, 8939 – 8949.*

(28) Ulrich, S.; Seijo, M.; Laguecir, A.; Stoll, S. Nanoparticle adsorption on a weak polyelectrolyte. Stiffness, pH, charge mobility, and ionic concentration effects investigated by Monte Carlo simulations. Journal of Physical Chemistry B **2006***, 110, 20954–20964.*

(29) Carnal, F.; Stoll, S. Adsorption of weak polyelectrolytes on charged nanoparticles. Impact of salt valency, pH, and nanoparticle charge density. Monte Carlo simulations. Journal of Physical Chemistry B **2011***, 115, 12007–12018.*

(30) Ulrich, S.; Seijo, M.; Carnal, F.; Stoll, S. *Formation of complexes between nanoparticles and weak polyampholyte chains. Monte Carlo simulations.* Macromolecules **2011**, *44, 1661–1670.*

(31) Reed, C. E.; Reed, W. F. *Monte Carlo study of titration of linear polyelectrolytes.* Journal of Chemical Physics **1992**, *96, 1609–1620.*

(32) Ullner, M. *In* Handbook of Polyelectrolytes and Their Applications*; Tripathy, S. K., Kumar, J, Nalwa, H. S., Eds.; American Scientific Publishers, 2002; Vol. 3 ch. 10, pp. 271–308.*

(33) Reščič, J.; Linse, P. *Molsim: A modular molecular simulation software.* Journal of Computational Chemistry **2015**, *36, 1259–1274.*

(34) Dias, R. S.; Pais, A. A.; Miguel, M. G.; Lindman, B. *Modeling of DNA compaction by polycations.* Journal of Chemical Physics **2003**, *119, 8150–8157.*

(35) Nguyen, T. T.; Shklovskii, B. I. *Overcharging of a macroion by an oppositely charged polyelectrolyte.* Physica A **2001**, *293, 324–338.*

Graphical TOC Entry